Polyphyllin II regulates ROS levels and promotes ferroptosis in bladder cancer cells

QUANLAI QIAO[1], RUIFANG GUO[2], ZHONGHUA SUN[1], YAXIN SHI[3], YUNING XIE[4] and ZHIYONG LIU[5,6]

[1]Medical Department, Affiliated Hospital of Shandong University of Traditional Chinese Medicine, Jinan, Shandong 250014, P.R. China; [2]Department of Geriatric Medicine, Affiliated Hospital of Shandong University of Traditional Chinese Medicine, Jinan, Shandong 250014, P.R. China; [3]First Clinical Medical College, Shandong University of Traditional Chinese Medicine, Jinan, Shandong 250355, P.R. China; [4]Clinical Study Center, Affiliated Hospital of Shandong University of Traditional Chinese Medicine, Jinan, Shandong 250014, P.R. China; [5]Central Laboratory, Affiliated Hospital of Shandong University of Traditional Chinese Medicine, Jinan, Shandong 250014, P.R. China; [6]Shandong Key Laboratory of Dominant Diseases of Traditional Chinese Medicine, Jinan, Shandong 250014, P.R. China.

Received May 29, 2025; Accepted November 21, 2025

DOI: 10.3892/mmr.2026.13858

Abstract. Bladder cancer is a challenging disease with high recurrence rates and limited treatment options. Studies have highlighted the role of ferroptosis, an iron-dependent cell death mechanism, in cancer progression and treatment. In the present study, the regulatory mechanisms of polyphyllin II (PPII) on ferroptosis in bladder cancer cells were investigated. Cell viability and colony formation assays demonstrated that PPII effectively inhibited the proliferation of bladder cancer cells. RNA sequencing analysis revealed differentially expressed genes upon PPII treatment, with Cluster 6 exhibiting dose-dependent expression changes. Gene Ontology and pathway enrichment analyses revealed enrichment of ferroptosis-related pathways. PPII treatment markedly increased reactive oxygen species (ROS) levels and promoted Fe^{2+} accumulation in bladder cancer cells. Additionally, PPII downregulated the expression of glutathione peroxidase 4 (GPX4), a key regulator of ferroptosis. These findings indicate that PPII promotes ferroptosis in bladder cancer cells through the modulation of ROS levels and GPX4 activity. Further investigations into the molecular mechanisms and potential combination therapies are warranted.

Correspondence to: Professor Zhiyong Liu, Central Laboratory, Affiliated Hospital of Shandong University of Traditional Chinese Medicine, 16369 Jingshi Road, Lixia, Jinan, Shandong 250014, P.R. China
E-mail: zhiyonglq@163.com

Dr Yuning Xie, Clinical Study Center, Affiliated Hospital of Shandong University of Traditional Chinese Medicine, 16369 Jingshi Road, Lixia, Jinan, Shandong 250014, P.R. China
E-mail: xyn0634@gmail.com

Key words: bladder cancer, ferroptosis, polyphyllin II, reactive oxygen species, lipid peroxidation, glutathione peroxidase 4

Introduction

Bladder cancer is among the most common malignancies of the urinary system worldwide, with an estimated 614,000 new cases and nearly 220,000 related deaths globally in 2022 (1). Bladder cancer is divided into non-muscle-invasive (NMIBC) and muscle-invasive (MIBC) subtypes. Although NMIBC has an improved prognosis, it necessitates costly long-term monitoring, and ~20% of cases progress to MIBC. The high incidence and recurrence rates of bladder cancer make it one of the most challenging diseases in the field of urology. While early detection and treatment can markedly improve patient outcomes, the prognosis for those with invasive or metastatic disease remains poor. Although traditional therapeutic approaches, such as surgery, radiation therapy, and chemotherapy, are effective to some extent in delaying disease progression, they are often limited by significant side effects, suboptimal efficacy, and the development of drug resistance (2,3). As a result, the development of novel therapeutic agents to improve clinical outcomes for bladder cancer patients, reduce disease recurrence, and mitigate treatment-related toxicity is urgently needed.

Ferroptosis is an iron-dependent cell death mechanism driven by lipid peroxidation and shows promise for treating cancers resistant to conventional therapies. Nevertheless, the therapeutic potential of ferroptosis induction in bladder cancer remains unclear (4). The identification of ferroptosis-inducing factors and the exploration of their underlying mechanisms have emerged as promising research directions. For instance, cirSIRT5 has been shown to promote ferroptosis in bladder cancer (5) and abietic acid was also reported to induce ferroptotic cell death in this malignancy (6).

Reactive oxygen species (ROS) play a central role in inducing ferroptosis by promoting lipid peroxidation, leading to cellular damage and death (7). In this context, the glutathione peroxidase 4 (GPX4) enzyme is a key regulator, as it protects cells from ROS-induced lipid peroxidation (8). The dysregulation of GPX4 has been associated with increased susceptibility to ferroptosis, making it a critical target in cancer therapy (9). Targeting the ferroptosis pathway, particularly through the modulation of ROS levels and GPX4 activity, represents a promising therapeutic

strategy for the treatment of bladder cancer, as it offers a novel approach for overcoming the limitations of conventional therapies and addressing drug resistance (10).

Traditional Chinese medicine (TCM) and its bioactive components have garnered significant attention because of their role in modulating ferroptosis, offering new strategies for cancer treatment (11). Among these compounds, *Paris polyphylla* and its polyphyllin constituents have been reported to exert antitumor effects by promoting ferroptosis through various mechanisms. For example, research has shown that polyphyllin I (PPI) can induce ferroptosis by downregulating GPX4 expression and accumulating ROS, which triggers inhibitory effects on the proliferation, invasion and metastasis of hepatocellular carcinoma cells (12). Additionally, polyphyllin III has been shown to deplete GPX4 levels, accumulate ROS and induce ferroptosis in breast cancer cells (13). Despite these findings, the specific role of polyphyllin II (PPII) in regulating ferroptosis in bladder cancer remains unexplored. The sequencing results of the present study suggested that PPII may regulate the ROS levels and ferroptosis in bladder cancer. In addition, GPX4 is a key regulatory factor for ferroptosis. Therefore, it was hypothesized that PPII is likely to promote ROS accumulation, cause Fe^{2+} overload by downregulating GPX4 levels, and ultimately induce ferroptosis.

Materials and methods

Cell culture. MIBC (T24 and 5637) provided by Professor Shengtian Zhao (First Clinical Medical College, Qilu Hospital of Shandong University, Jinan, Shandong) were used in the present study. The T24 and 5637 cell lines are both well-established models of MIBC and share a common TP53 mutation background. Using two distinct cell lines helps demonstrate that the observed pro-ferroptotic effect of PPII is not an isolated phenomenon limited to a single genetic context but can be reproduced across different models of MIBC. The cells were cultured in RPMI-1640 medium (cat. no. CM10041, Macgene Technology Ltd.) supplemented with 10% fetal bovine serum (cat. no. 10270-106; Gibco; Thermo Fisher Scientific, Inc.). The two cell lines were maintained at 37˚C in a humidified incubator with 5% CO_2.

Cell viability assay. Cell viability was assessed using a CCK-8 assay kit (E-CK-A362, Elabscience Bionovation Inc.). T24 ($3x10^3$) and 5637 ($6x10^3$) cells were seeded into 96-well plates and incubated at 37˚C with 5% CO_2 overnight, after which the cells were treated with cisplatin or PPII. Following treatment, 10% CCK-8 solution was added to each well and gently mixed, and the plates were then incubated for an additional 2 h. The absorbance was measured at 450 nm using a spectrophotometer (Type 1510; Thermo Fisher Scientific, Inc.).

Colony formation assay. To assess the proliferative capacity of the cells, a colony formation assay was performed. Cells (800 cells/well) treated with gradient concentrations of PPII (0-0.8 μM) were seeded into six-well plates and cultured in medium supplemented with 10% fetal bovine serum, after which they were allowed to grow at 37˚C with 5% CO_2 for 10 days until visible colonies formed. The cells were then gently washed with PBS and fixed with 4% paraformaldehyde for 15 min at room temperature (RT). After fixation, the colonies were stained with 0.1% crystal violet for 30 min at RT, followed by rinsing with water to remove excess dye. The number of stained colonies was counted to evaluate the clonogenic potential of the cells.

RNA-sequencing and data pre-processing. T24 cells were treated with gradient concentrations of PPII [0 (NC group), 0.2 (L group) and 0.4 (H group) μM] for 48 h and total RNA were extracted with a MJzol animal RNA Extraction Kit (cat. no. Majorbio) following by the manufacturer's protocol. RNA quality and integrity were analyzed using a NanoPhotometer spectrophotometer (Implen GmbH) and an Agilent 2100 Bioanalyzer (Agilent Technologies, Inc.). To construct RNA-seq libraries, ribosomal RNA (rRNA) was removed from total RNA, and the remaining mRNA was then randomly fragmented. The RNA-seq libraries were constructed using an Illumina Truseq RNA Sample Prep Kit (Illumina, Inc.) and sequenced on a NovaSeq 6000 system (Illumina, Inc.). Prior to bioinformatics analysis, FastQC (http://www.bioinformatics.babraham.ac.uk/projects/fastqc/) was used to assess the quality of the raw data and the raw data were preprocessed to obtain high-quality clean read data. Cleaned reads were then mapped to the human reference genome GRCh38/hg38 using the spliced-read aligner HISAT2 (14) and StringTie (15) to obtain raw read counts and transcripts per million (TPM).

Gene expression and dynamic expression model analyses. Raw read count data were used for gene expression analyses. Genes with low counts might represent a sequencing bias and contribute less to further analysis; thus, genes with zero expression values were excluded. After data filtering, differential expression analysis was performed with the Bioconductor package DESeq2 (16). Any gene with a P-value <0.05 and a fold change >1.25 was regarded as a significantly differentially expressed gene (DEG).

TPM of DEGs were used for c-means clustering with the R package Mfuzz to characterize dynamic changes in expression patterns (17). Fuzzy c-means (FCM) clustering is a soft clustering method performed with the Mfuzz algorithm with two key parameters (c=number of clusters and m=fuzzification parameter). The algorithm iteratively assigns the profile to the cluster with the shortest Euclidean distance while minimizing any objective function. In the present study, the data were clustered with the parameters c=10 and m=2.

Pathway enrichment and Gene Ontology (GO) analysis. GO functional enrichment and Kyoto Encyclopedia of Genes and Genomes (KEGG) pathway analyses were performed using the R package clusterProfiler (18). GO terms were divided into three separate subgroups: Molecular functions (MFs), cellular components (CCs) and biological processes (BPs). Enriched GO terms and KEGG pathways were identified according to the cutoff criterion of P-values <0.05.

Immunoblotting. Western blotting was carried out following described protocols (19). Briefly, total cellular proteins were extracted using RIPA lysis buffer (cat. no. P0013C; Beyotime Biotechnology), and their concentrations were quantified with a BCA assay kit (cat. no. P0010S; Beyotime Biotechnology).

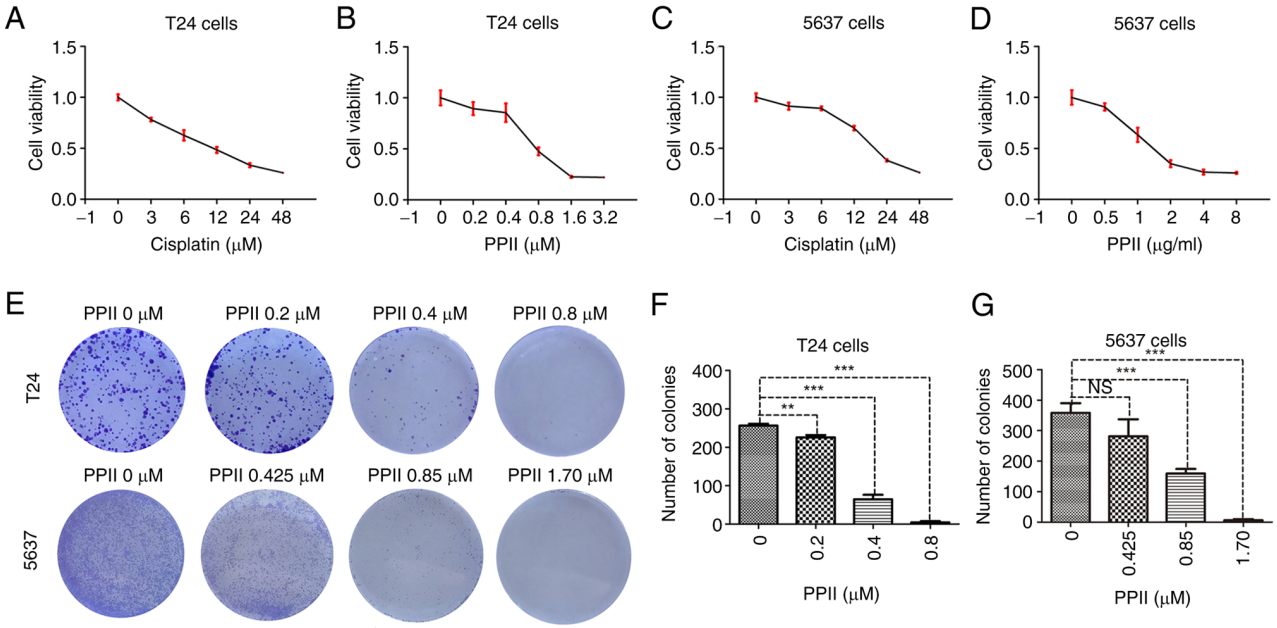

Figure 1. PPII inhibits the viability and colony formation of BC cells. A CCK-8 assay kit was used to assess the effects of cisplatin and PPII on the viability of (A and B) T24 and (C and D) 5637 cells, respectively. (E) Representative images showing the inhibitory effect of PPII on BC cell colony formation and (F and G) display the statistical analysis of colony numbers. NS, no significant difference, **P<0.01 and ***P<0.001. PPII, polyphyllin II; BC, bladder cancer.

An equal amount of protein (20 μg per lane) was separated by 10% SDS-PAGE gel and subsequently electrophoretically transferred onto a PVDF membrane (cat. no. IPVH00010; MilliporeSigma). The membrane was blocked with 5% skimmed milk powder in TBST buffer (0.1% Tween-20) at RT for 1 h and then probed with the primary antibody at 4˚C overnight. After washing, it was incubated with an HRP-conjugated goat anti-mouse secondary antibody (1:3,000 for GPX4 and 1:10,000 for ACTB; cat. no. A0216; Beyotime Biotechnology) at RT for 1 h. Finally, the target protein bands were visualized using an enhanced chemiluminescence (ECL) substrate. The primary antibodies used in the present study included GPX4 (mouse-sourced antibody, 1:1,000; cat. no. 67763-1-Ig) (20) purchased from Proteintech Group, Inc. and ACTB (mouse-sourced antibody, 1:10,000; cat. no. A5441) (21), which was obtained from Sigma-Aldrich (Merck KGaA). The intensity of the protein bands was quantified using ImageJ (version 1.53q; National Institutes of Health).

ROS detection analysis. Intracellular ROS levels were determined using a Reactive Oxygen Species Assay Kit (cat. no. S0033S; Beyotime Biotechnology), with DCFH-DA as the primary reagent. In brief, T24 and 5637 cells were plated in 6-well plates and treated with gradient concentrations of PPII (0, 0.4 and 0.8 μM for T24 cells and 0, 0.85 and 1.70 μM for 5637 cells) for 48 h. After treatment, the cells were incubated with DCFH-DA for 30 min at 37˚C and the nuclei were stained with Hoechst 33342 (cat. no. C1029; Beyotime Biotechnology) for 10 min. The fluorescence was then visualized using a fluorescence microscope (Vert.A1; Zeiss GmbH) and the mean fluorescence intensity was quantified using ImageJ (version 1.53q; National Institutes of Health).

Fe^{2+} detection analysis. Fe^{2+} detection was performed according to the FerroOrange manufacturer's instructions (cat. no. F374; Dojindo Laboratories, Inc.). After 48 h of PPII treatment with various concentrations of PPII (as described in the ROS detection analysis section), the culture medium was removed and the BC cells were washed three times with HBSS. The cells were then incubated with FerroOrange working solution (1 μM) at 37˚C in a 5% CO_2 atmosphere for 30 min. Changes in fluorescence intensity were observed using a fluorescence microscope (Vert.A1; Zeiss GmbH).

Analysis of oxidative stress-related markers. T24 and 5637 cells were treated as aforementioned, followed by washing with PBS and lysis with lysis buffer. After centrifugation (19,480 x g), the supernatant was collected for the detection of malondialdehyde (MDA) levels using a MDA detection kit (cat. no. S0131S; Beyotime Biotechnology). The absorbance at 532 nm was measured with a spectrophotometer (Type 1510; Thermo Fisher Scientific, Inc.). Similarly, superoxide dismutase (SOD) levels were measured following the instructions of the corresponding reagent kit (cat. no. S0101M; Beyotime Biotechnology), with the absorbance recorded at 450 nm.

Detection of oxidized and non-oxidized lipids. T24 and 5637 cells were treated with gradient concentrations of PPII for 48 h as aforementioned. The medium was then replaced with complete medium containing BODIPY 581/591 C11 (10 μM; cat. no. D3861; Invitrogen; Thermo Fisher Scientific, Inc.) and the cells incubated at 37˚C with 5% CO_2 for an additional 30 min. The cells were then washed three times with PBS (5 min per wash), followed by staining with Hoechst 33342 for 10 min at 37˚C. After the samples were washed, the fluorescence intensities of oxidized and non-oxidized lipids were observed under a fluorescence microscope (Vert.A1; Zeiss GmbH), and the mean fluorescence intensity was quantified using ImageJ (version 1.53q; National Institutes of Health).

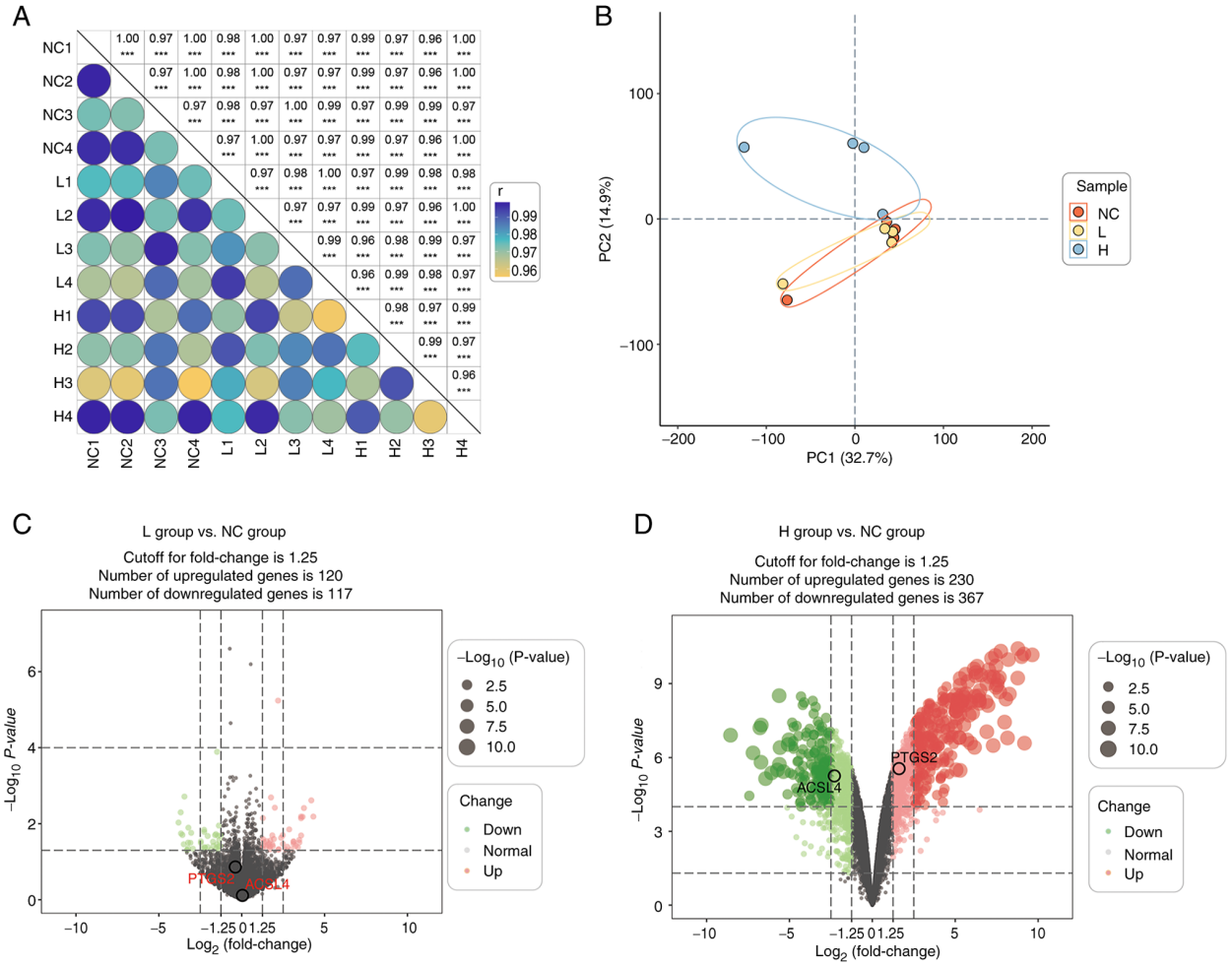

Figure 2. Homogeneity analysis of transcriptome sequencing and visualization of intergroup gene differences. Homogeneity analysis was conducted on sequencing samples from different groups, with results displayed as (A) heatmaps and (B) coordinate plots. (C) Differential gene expression between the low-concentration PPII group (L) and the NC, as well as between (D) the high-concentration PPII group (H) and the NC are shown in MA plots. ***P<0.001. NC, control group; PPII, polyphyllin II.

Statistical analysis. All the statistical analyses were performed using GraphPad Prism (version 5.0; Dotmatics). Data are presented as the mean ± standard deviation (SD) from at least three independent experiments. For comparisons between two groups, an unpaired two-tailed Student's t-test was used. For comparisons among more than two groups, one-way analysis of variance (ANOVA) was performed, followed by Dunnett's test for multiple comparisons when all groups were compared against a single control group. DEGs were identified using an adjusted P-value (False Discovery Rate; FDR) threshold. Furthermore, Pearson correlation analysis was conducted using R software (version 4.3.0; https://cran.r-project.org/bin/windows/base/old/4.3.0/) to assess the relationships between oxidative stress indicators. P<0.05 was considered to indicate a statistically significant difference.

Results

PPII inhibits the cell viability and colony formation of BC cells. The effect of PPII on bladder cancer cell viability was assessed using a CCK-8 assay. T24 and 5637 cells were treated with increasing concentrations of cisplatin (used as a positive control, Fig. 1A and C) or PPII (Fig. 1B and D) for 48 h. The CCK-8 results revealed that PPII could inhibited the viability of bladder cancer cells and the calculated IC_{50} values of cisplatin were 11.70±1.31 μM for T24 cells and 20.17±0.82 μM for 5637 cells, whereas the IC_{50} values of PPII were 0.86±0.09 μM for T24 cells and 1.72±0.21 μM for 5637 cells.

The effect of the PPII on the proliferative capacity of bladder cancer cells was evaluated through colony formation assays. The results suggested that PPII effectively reduced the number of colonies formed by T24 and 5637 cells in a dose-dependent manner (Fig. 1E). Statistical analysis revealed that 0.2, 0.4, and 0.8 μM PPII significantly decreased the number of colonies formed by T24 cells (P<0.01, Fig. 1F). Similarly, PPII at concentrations of 0.85 and 1.70 μM PPII markedly inhibited colony formation in 5637 cells (P<0.001, Fig. 1G).

RNA sequencing analysis of BC cells treated with PPII. Previous experiments had indicated that PPII effectively inhibits the proliferation of BC cells. To minimize the confusing effects of cytotoxicity from high concentrations of drugs, the present study chose PPII drug concentrations (0, 0.2, and 0.4 μM) that did not affect T24 cell viability for RNA transcriptome sequencing (Fig. S1A), aiming to elucidate the potential mechanisms involved in this process.

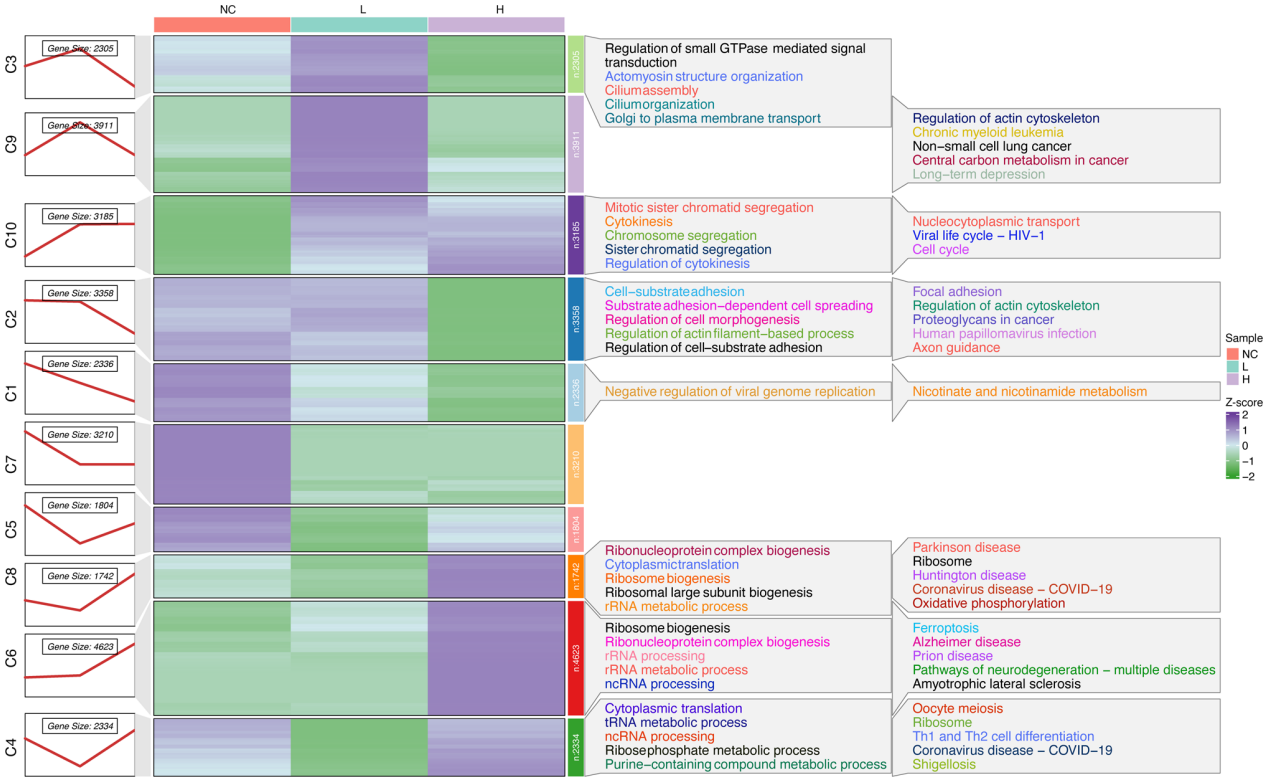

Figure 3. Dynamic changes in gene expression profiles in T24 cells during the progression of PPII treatment. Expression profiles and subcluster distributions of genes in T24 cells were analyzed following PPII treatment. PPII, polyphyllin II.

Overview of the transcriptomic analysis. T24 cells were treated with high-concentration and low-concentration PPII for 48 h, after which the RNA was harvested in quadruplicate. A total of 12 samples were divided into three groups, namely, the NC, L and H groups, according to the concentrations of PPII (Fig. 2A). DEGs between each group were identified using a P-value <0.05 and a fold change greater than the cutoff. A total of 834 DEGs were identified between the NC, L and H groups. Principal components analysis revealed that the between-group samples were clearly separated from each other and revealed good clustering of samples within the same group, indicating distinct gene expression profiles upon PPII treatment (Fig. 2B). Volcano plots also revealed the DEGs that differed from each other in the groups (Fig. 2C and D). All the DEGs were included in the subsequent analyses.

Identification of dynamic expression patterns. To understand the dynamic alteration expression profiles in T24 cells during the progression of PPII treatment, 834 DEGs were subjected to soft clustering to determine their expression trends in the three series groups. The DEGs were divided into 10 clusters according to their trend similarity over time using a soft Mfuzz clustering algorithm and not all the clusters exhibited consistent expression trends with a distinct peak. A heatmap revealed that both Cluster 6 and Cluster 8 showed transcriptional upregulation response to PPII treatment, Cluster 6 demonstrated a more consistent concentration-dependent pattern, showing gradual upregulation with increasing PPII concentrations. By contrast, Cluster 8 exhibited a biphasic response with initial downregulation at lower concentrations followed by upregulation at higher doses (Fig. 3). On the basis of this clear concentration-dependent response, Cluster 6 was selected for further investigation.

GO and KEGG analyses of Cluster 6. GO and KEGG pathway analyses of the DEGs in Cluster 6 revealed enrichment of ribosome-related and RNA processing-related categories in the GO analysis (Fig. 4A). KEGG analysis revealed pathways related to ferroptosis and ROS (Fig. 4B), and ferroptosis-related factors, including PTGS2 and ACSL4, showed varying degrees of changes with dose-dependent manner in volcano maps (Fig. 2C and D). Given that ferroptosis is closely associated with the regulation of cell proliferation and that ROS play a crucial role in the ferroptosis process, subsequent experiments focused on validating the regulatory effects of PPII on ROS and ferroptosis.

PPII promotes ROS in BC cells. The effect of PPII on ROS levels in bladder cancer cells was assessed using a ROS detection kit, as detailed in the methods section. The fluorescence intensity was used to quantify the ROS levels, revealing that T24 cells exhibited a significant increase in fluorescence intensity following PPII treatment. Notably, the fluorescence intensity in the 0.8 μM PPII treatment group was comparable to that in the positive control group (CRTL + Rosup; Fig. 5A). Statistical analysis demonstrated that as the concentration of PPII increased, the average fluorescence intensity significantly increased (Fig. 5C; P<0.001) in a dose-dependent manner. Similar results were observed in 5637 cells (Fig. 5B and C). Since MDA and SOD are critical regulators of ROS levels, their concentrations were measured. High concentrations of PPII (0.8 μM for T24 cells and 1.70 μM for 5637 cells) significantly increased MDA levels (Fig. 5D, P<0.05) but inhibited SOD activity (Fig. 5E; P<0.05).

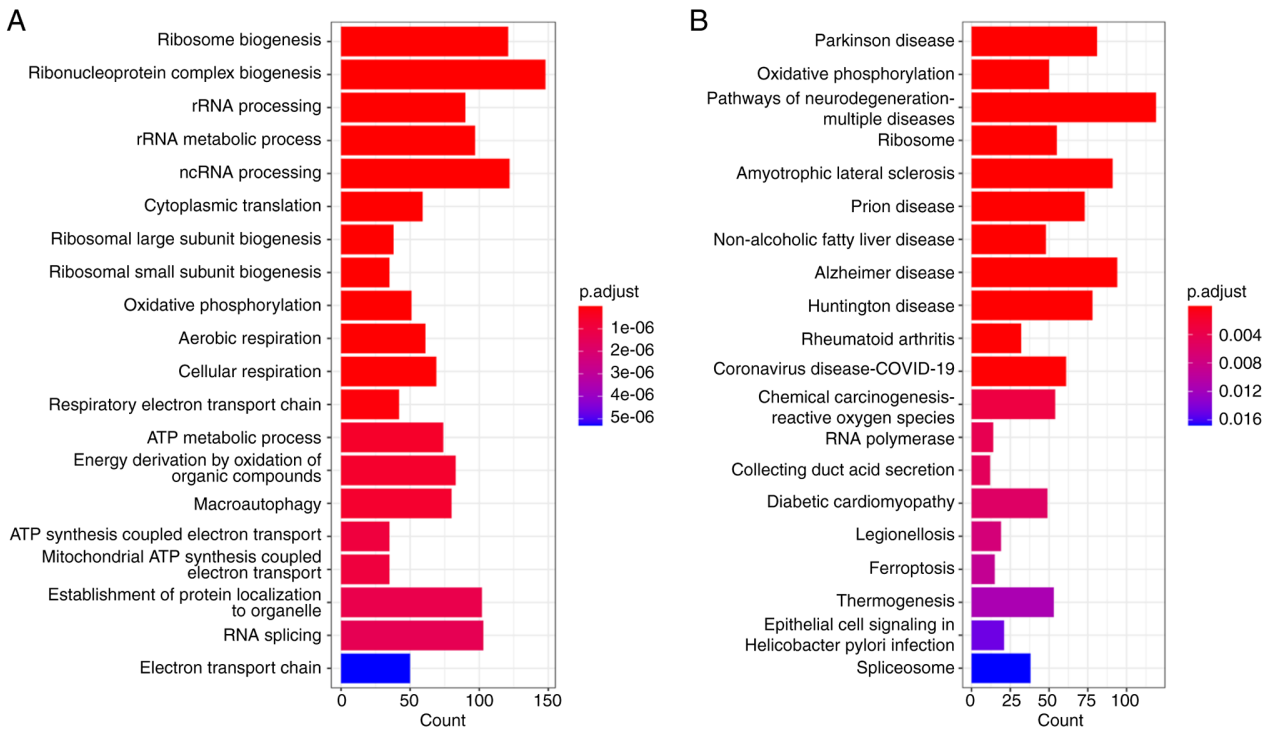

Figure 4. GO and KEGG Analysis. Differentially expressed genes in Cluster 6 were analyzed using (A) GO and (B) KEGG pathways. GO, Gene Ontology; KEGG, Kyoto Encyclopedia of Genes and Genomes.

Furthermore, Pearson analysis revealed a negative correlation between ROS and SOD, whereas ROS and MDA showed a positive correlation (Fig. S1B). These findings suggested that PPII effectively increases ROS levels in bladder cancer cells.

PPII promotes ferroptosis in BC cells. Fe^{2+} accumulation is a key indicator of ferroptosis. To assess changes in Fe^{2+} levels after PPII treatment in BC cells, the FerroOrange kit was used. The results revealed that the Fe^{2+} staining intensity increased with increasing PPII concentration in T24 cells (Fig. 6A). Statistical analysis revealed that the average fluorescence intensity significantly increased in a dose-dependent manner (Fig. 6B; $P<0.001$). Consistent findings were also observed in 5637 cells (Fig. 6C and D).

The accumulation of oxidized lipids serves as a key marker in the process of ferroptosis. Using specific probes, the levels of both oxidized and non-oxidized lipids was assessed. Treatment with 0.8 μM PPII significantly elevated the levels of oxidized lipids in T24 cells ($P<0.05$), but did not markedly affect the levels of non-oxidized lipids (Fig. 6E and F). Similarly, in 5637 cells, treatment with 0.85 μM and 1.70 μM PPII markedly increased oxidized lipid levels (Fig. 6G and H).

Molecular docking suggests that PPII and GPX4, a key regulatory factor of Ferroptosis, have potential good binding ability (Fig. S1C and D; binding energy, -8.7 kcal/mol). Further analysis of the expression of GPX4 was conducted using western blotting. The results indicated that treatment with high concentrations of PPII markedly decreased GPX4 levels in both T24 and 5637 cells (Fig. 6I and J). Furthermore, PPII reduces the increase in GPX4 levels caused by the ferroptosis inhibitor Fer-1 (Fig. S1E). These findings suggested that the regulatory effect of PPII on ferroptosis is mediated by GPX4.

Discussion

ROS play pivotal roles in ferroptosis, a form of programmed cell death characterized by iron-dependent lipid peroxidation (22). Fe^{2+} is crucial in this process, serving as a catalyst in the Fenton reaction, which converts hydrogen peroxide into highly active hydroxyl radicals. These radicals exacerbate oxidative stress by promoting the peroxidation of polyunsaturated fatty acids within cellular membranes (23). The resulting accumulation of oxidized lipids leads to cellular damage and ultimately triggers ferroptosis (24). This relationship between Fe^{2+} and ROS underscores the importance of iron metabolism in the regulation of ferroptosis, particularly in cancer cells in which these pathways are often dysregulated (10,25).

The antioxidant enzyme GPX4 plays a critical role in counteracting oxidative stress. By reducing lipid hydroperoxides to their corresponding alcohols, GPX4 prevents the propagation of lipid peroxidation and protects cells from ferroptosis (26). However, when GPX4 activity is compromised, either through genetic downregulation or pharmacological inhibition, cells become more susceptible to ferroptosis because of the unchecked accumulation of ROS and oxidized lipids (27).

According to the *Chinese Pharmacopoeia*, the Polyphyllins, including PPI, PPII, Polyphyllin VI (PPVI), and Polyphyllin VII (PPVII), are the major active compounds used for the authentication of *Paris polyphylla*. Our previous experimental data indicated that, among these compounds, compared with PPI, PPVI, and PPVII, PPII has superior efficacy in inhibiting the viability of both T24 and 5637 cells (28). In the present study, PPII treatment markedly downregulated GPX4 expression, leading to elevated ROS levels and increased lipid peroxidation in bladder cancer cells. These findings suggest

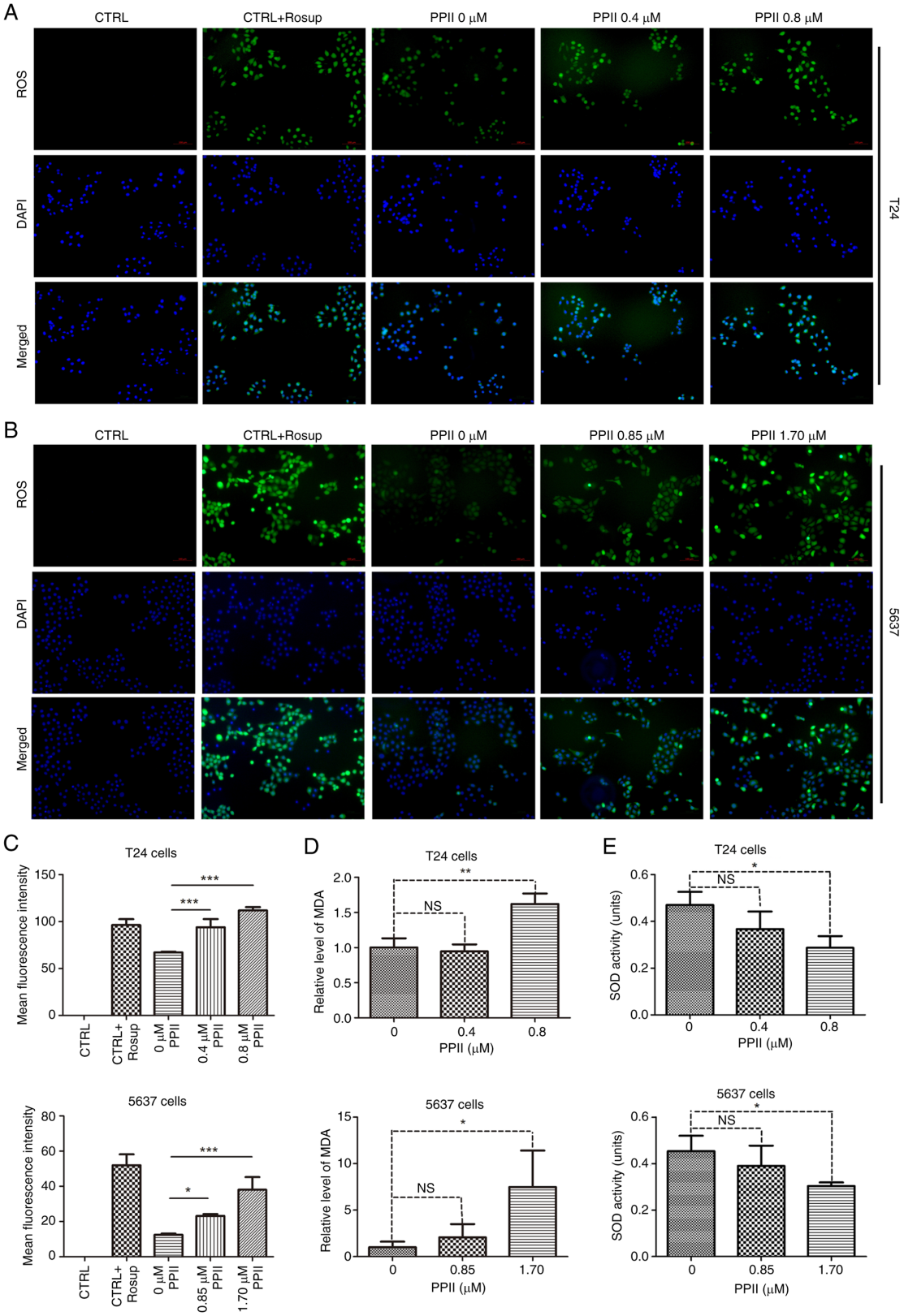

Figure 5. ROS level detection. (A) T24 and (B) 5637 cells (magnification, x100) were treated with gradient concentrations of PPII and (C) their ROS levels were measured using a reagent kit, with the average fluorescence intensity analyzed statistically. The levels of (D) MDA and (E) SOD in BC cells were determined using the corresponding assay kits as described in the methods section. NS, no significant difference, *P<0.05, **P<0.01 and ***P<0.001. ROS, reactive oxygen species; PPII, polyphyllin II; MDA, malondialdehyde; SOD, superoxide dismutase; BC, bladder cancer.

that PPII may promote ferroptosis by disrupting the delicate balance between ROS production and antioxidant defense mechanisms mediated by GPX4.

In addition to GPX4, other oxidative stress-related markers, such as MDA and SOD, play significant roles in the regulation of ferroptosis. MDA is a byproduct of lipid peroxidation and serves

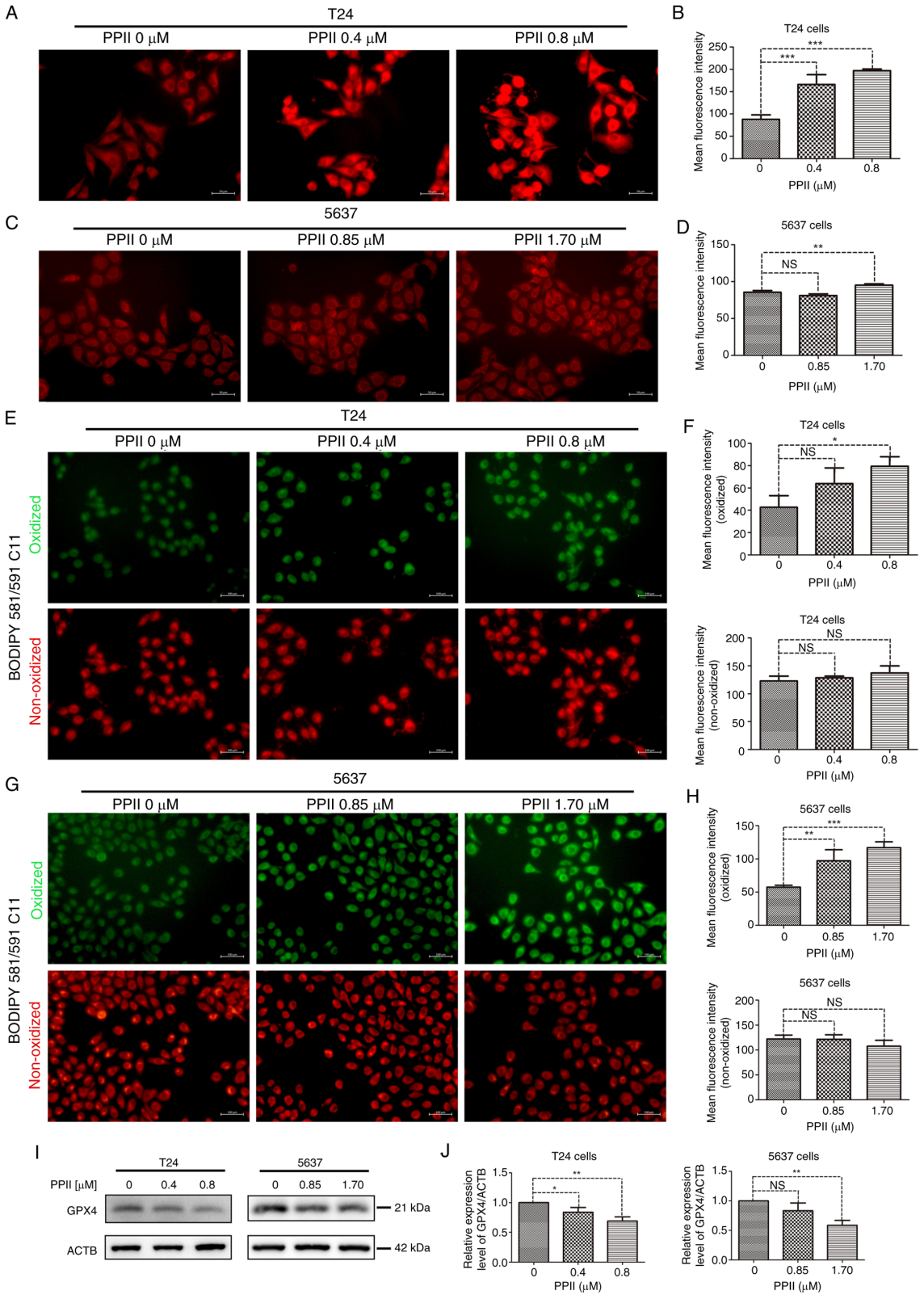

Figure 6. PPII promotes the accumulation of iron ions and oxidized lipids in BC cells. Fe^{2+} levels in (A) T24 and (C) 5637 cells were measured using the FerroOrange assay kit (magnification, x200) and (B and D) the average fluorescence intensity was statistically analyzed. (E and G) The levels of oxidized and non-oxidized lipids were detected using the BODIPY 581/591 C11 assay kit (magnification, x100) and (F and H) subsequently analyzed. (I) GPX4 levels were assessed by immunoblotting and (J) grayscale analysis, n=3 independent experiments. NS, no significant difference; *P<0.05; **P<0.01, ***P<0.001 vs. control group (0 μM). GPX4, glutathione peroxidase 4; PPII, polyphyllin II.

as a biomarker for oxidative stress (29). The present study revealed that PPII treatment leads to increased MDA levels in the bladder cancer cells, indicating increased lipid peroxidation. Conversely, the activity of SOD, an enzyme responsible for detoxifying superoxide radicals (30), was inhibited by PPII, contributing to the accumulation of ROS. These findings suggested that PPII

modulates multiple components of the oxidative stress pathway, promoting ferroptosis through both the upregulation of lipid peroxidation and the inhibition of antioxidant defenses.

The interplay between Fe^{2+}, ROS and lipid peroxidation is further complicated by the involvement of various signaling pathways. For instance, ROS can activate signaling cascades that promote the expression of pro-ferroptotic genes, whereas Fe^{2+}-mediated lipid peroxidation can amplify these signals, creating a feed-forward loop that drives ferroptosis (31,32). Additionally, the downregulation of GPX4 disrupts redox homeostasis, tipping the balance in favor of oxidative stress and ferroptosis (33). The present study highlighted the potential of targeting this axis in bladder cancer therapy. While the initial transcriptomic profiling was conducted in T24 cells as a resource-efficient hypothesis-generating step, all key mechanistic findings, particularly regarding ROS accumulation and ferroptosis activation, were rigorously validated in both T24 and 5637 cell lines. This dual-cell-line validation approach ensures that the conclusions of the present study about PPII's pro-ferroptotic effects are generalizable across different MIBC models, as PPII-induced GPX4 downregulation, combined with increased Fe^{2+} accumulation and ROS production, leads to a potent ferroptotic response in bladder cancer cells. Although PPII affects the ferroptosis process of bladder cancer cells through GPX4, GPX4 may not be the direct target of PPII. Fe ions not only participate in the induction of ferroptosis but also cause pyroptosis (34). Does the PPII regulate the accumulation of Fe ions to induce other forms of cell death? It is hoped to clarify the upstream regulatory factors through which PPII affects ferroptosis through GPX4, such as Nrf2/HO-1 pathway, in future studies and explore other forms of cell death induced by PPII.

In conclusion, the promotion of ferroptosis through the modulation of Fe^{2+} levels, ROS production, and lipid peroxidation represents a promising therapeutic strategy in bladder cancer. The downregulation of GPX4 by PPII and the associated increase in oxidative stress suggest that targeting the above processes could be an effective approach for increasing ferroptosis. PPII is a potential small molecule drug for the treatment of bladder cancer and future studies should further investigate the molecular mechanisms underlying the effects of PPII and explore its potential in combination with other ferroptosis-inducing agents. Furthermore, *in vivo* validation and pharmacokinetic analysis should also be conducted.

Acknowledgements

The authors would like to thank Professor Shengtian Zhao (First Clinical Medical College, Qilu Hospital of Shandong University, Jinan, Shandong) for providing the T24 and 5637 cell lines.

Funding

The present study was funded by the Natural Science Foundation of Shandong Province, China (grant no. ZR2020QH337).

Availability of data and materials

The data generated in the present study are included in the figures of this article. The data generated in the present study may be found in the Genome Sequence Archive (Genomics, Proteomics & Bioinformatics, 2021) at the National Genomics Data Center (Nucleic Acids Research, 2022), China National Center for Bioinformation/Beijing Institute of Genomics, Chinese Academy of Sciences (GSA-Human: HRA005259; https://ngdc.cncb.ac.cn/gsa-human). The original images and analytical data may be found in the figshare repository and can be accessed via https://figshare.com/articles/dataset/Polyphyllin_II_regulates_ROS_levels_and_promotes_ferroptosis_in_bladder_cancer_cells/30448508.

Authors' contributions

ZL and YX conceived and designed the study. QQ and YS conducted the experiments. Data analysis and display (writing the R language code for the bioinformatics analysis and for generating the figures in the article) were performed by ZS and RG. RG and ZS confirm the authenticity of all the raw data. All authors participated in the manuscript writing which was ultimately edited by YX and ZL. All authors read and approved the final manuscript.

Ethics approval and consent to participate

The T24 and 5637 cell lines used in this experiment were approved by the Ethics Committee of the Affiliated Hospital of Shandong University of Traditional Chinese Medicine.

Patient consent for publication

Not applicable.

Competing interests

The authors declare that they have no competing interests.

References

1. Bray F, Laversanne M, Sung H, Ferlay J, Siegel RL, Soerjomataram I and Jemal A: Global cancer statistics 2022: GLOBOCAN estimates of incidence and mortality worldwide for 36 cancers in 185 countries. CA Cancer J Clin 74: 229-263, 2024.
2. Li F, Zhang H, Huang Y, Li D, Zheng Z, Xie K, Cao C, Wang Q, Zhao X, Huang Z, *et al*: Single-cell transcriptome analysis reveals the association between histone lactylation and cisplatin resistance in bladder cancer. Drug Resist Updat 73: 101059, 2024.
3. Li F, Zheng Z, Chen W, Li D, Zhang H, Zhu Y, Mo Q, Zhao X, Fan Q, Deng F, *et al*: Regulation of cisplatin resistance in bladder cancer by epigenetic mechanisms. Drug Resist Updat 68: 100938, 2023.
4. Liu T, Xu X, Li J, Bai M, Zhu W, Liu Y, Liu S, Zhao Z, Li T, Jiang N, *et al*: ALOX5 deficiency contributes to bladder cancer progression by mediating ferroptosis escape. Cell Death Dis 14: 800, 2023.
5. Li W, Ou Y, Ye F, Cheng Z, Chen Z, Zhou Q, Yan X and Jiang H: cirSIRT5 induces ferroptosis in bladder cancer by forming a ternary complex with SYVN1/PHGDH. Cell Death Discov 10: 391, 2024.
6. Xu Y, Tong Y, Lei Z, Zhu J and Wan L: Abietic acid induces ferroptosis via the activation of the HO-1 pathway in bladder cancer cells. Biomed Pharmacother 158: 114154, 2023.
7. Wang B, Wang Y, Zhang J, Hu C, Jiang J, Li Y and Peng Z: ROS-induced lipid peroxidation modulates cell death outcome: Mechanisms behind apoptosis, autophagy, and ferroptosis. Arch Toxicol 97: 1439-1451, 2023.
8. Wu S, Guo N, Xu H, Li Y, Sun T, Jiang X, Fu D, You T, Diao S, Huang Y and Hu C: Caveolin-1 ameliorates hepatic injury in non-alcoholic fatty liver disease by inhibiting ferroptosis via the NOX4/ROS/GPX4 pathway. Biochem Pharmacol 230: 116594, 2024.

9. Liu H, Schreiber SL and Stockwell BR: Targeting dependency on the GPX4 lipid peroxide repair pathway for cancer therapy. Biochemistry 57: 2059-2060, 2018.
10. Zhang C, Liu X, Jin S, Chen Y and Guo R: Ferroptosis in cancer therapy: A novel approach to reversing drug resistance. Mol Cancer 21: 47, 2022.
11. Qin L, Zhong Y, Li Y and Yang Y: TCM targets ferroptosis: Potential treatments for cancer. Front Pharmacol 15: 1360030, 2024.
12. Yang R, Gao W, Wang Z, Jian H, Peng L, Yu X, Xue R, Peng W, Li K and Zeng P: Polyphyllin I induced ferroptosis to suppress the progression of hepatocellular carcinoma through activation of the mitochondrial dysfunction via Nrf2/HO-1/GPX4 axis. Phytomedicine 122: 155135, 2024.
13. Zhou Y, Yang J, Chen C, Li Z, Chen Y, Zhang X, Wang L and Zhou J: Polyphyllin III-Induced Ferroptosis in MDA-MB-231 Triple-negative breast cancer cells can be protected against by KLF4-Mediated upregulation of xCT. Front Pharmacol 12: 670224, 2021.
14. Kim D, Paggi JM, Park C, Bennett C and Salzberg SL: Graph-based genome alignment and genotyping with HISAT2 and HISAT-genotype. Nat Biotechnol 37: 907-915, 2019.
15. Pertea M, Pertea GM, Antonescu CM, Chang TC, Mendell JT and Salzberg SL: StringTie enables improved reconstruction of a transcriptome from RNA-seq reads. Nat Biotechnol 33: 290-295, 2015.
16. Love MI, Huber W and Anders S: Moderated estimation of fold change and dispersion for RNA-seq data with DESeq2. Genome Biol 15: 550, 2014.
17. Kumar L and Futschik M: Mfuzz: A software package for soft clustering of microarray data. Bioinformation 2: 5-7, 2007.
18. Wu T, Hu E, Xu S, Chen M, Guo P, Dai Z, Feng T, Zhou L, Tang W, Zhan L, *et al*: clusterProfiler 4.0: A universal enrichment tool for interpreting omics data. Innovation (Camb 2: 100141, 2021.
19. Shi YX, Xu L, Wang X, Zhang KK, Zhang CY, Liu HY, Ding P, Shi W and Liu Z: Paris polyphylla ethanol extract and polyphyllin I ameliorate adenomyosis by inhibiting epithelial-mesenchymal transition. Phytomedicine 127: 155461, 2024.
20. Zeng Y, Wu R, Wang F, Li S, Li L, Li Y, Qin P, Wei M, Yang J, Wu J, *et al*: Liberation of daidzein by gut microbial β-galactosidase suppresses acetaminophen-induced hepatotoxicity in mice. Cell Host Microbe 31: 766-780.e7, 2023.
21. Bayona C, Alza L, Ranđelović T, Sallán MC, Visa A, Cantí C, Ochoa I, Oliván S and Herreros J: Tetralol derivative NNC-55-0396 targets hypoxic cells in the glioblastoma microenvironment: An organ-on-chip approach. Cell Death Dis 15: 127, 2024.
22. Zi Y, Wang X, Zi Y, Yu H, Lan Y, Fan Y, Ren C, Liao K and Chen H: Cigarette smoke induces the ROS accumulation and iNOS activation through deactivation of Nrf-2/SIRT3 axis to mediate the human bronchial epithelium ferroptosis. Free Radic Biol Med 200: 73-86, 2023.
23. Henning Y, Blind US, Larafa S, Matschke J and Fandrey J: Hypoxia aggravates ferroptosis in RPE cells by promoting the Fenton reaction. Cell Death Dis 13: 662, 2022.
24. Pope LE and Dixon SJ: Regulation of ferroptosis by lipid metabolism. Trends Cell Biol 33: 1077-1087, 2023.
25. Zhao L, Zhou X, Xie F, Zhang L, Yan H, Huang J, Zhang C, Zhou F, Chen J and Zhang L: Ferroptosis in cancer and cancer immunotherapy. Cancer Commun (Lond) 42: 88-116, 2022.
26. Xie Y, Kang R, Klionsky DJ and Tang D: GPX4 in cell death, autophagy, and disease. Autophagy 19: 2621-2638, 2023.
27. Wang H, Cheng Y, Mao C, Liu S, Xiao D, Huang J and Tao Y: Emerging mechanisms and targeted therapy of ferroptosis in cancer. Mol Ther 29: 2185-2208, 2021.
28. Niu W, Xu L, Li J, Zhai Y, Sun Z, Shi W, Jiang Y, Ma C, Lin H, Guo Y and Liu Z: Polyphyllin II inhibits human bladder cancer migration and invasion by regulating EMT-associated factors and MMPs. Oncol Lett 20: 2928-2936, 2020.
29. Ye T, Yang W, Gao T, Yu X, Chen T, Yang Y, Guo J, Li Q, Li H and Yang L: Trastuzumab-induced cardiomyopathy via ferroptosis-mediated mitochondrial dysfunction. Free Radic Biol Med 206: 143-161, 2023.
30. Ji HS, Bang SG, Ahn MA, Kim G, Kim E, Eom SH and Hyun TK: Molecular cloning and functional characterization of heat Stress-responsive superoxide dismutases in garlic (Allium sativum L.). Antioxidants (Basel) 10: 815, 2021.
31. Liu J, Kang R and Tang D: Signaling pathways and defense mechanisms of ferroptosis. FEBS J 289: 7038-7050, 2022.
32. Wu ZF, Liu XY, Deng NH, Ren Z and Jiang ZS: Outlook of Ferroptosis-targeted lipid peroxidation in cardiovascular disease. Curr Med Chem 30: 3550-3561, 2023.
33. Zhang W, Liu Y, Liao Y, Zhu C and Zou Z: GPX4, ferroptosis, and diseases. Biomed Pharmacother 174: 116512, 2024.
34. Zhou B, Zhang JY, Liu XS, Chen HZ, Ai YL, Cheng K, Sun RY, Zhou D, Han J and Wu Q: Tom20 senses iron-activated ROS signaling to promote melanoma cell pyroptosis. Cell Res 28: 1171-1185, 2018.